Article

Validation of a Bar Linkage Model for Joint Angle Estimation During Cycling

Sien Dieltiens [1],*, Kurt Claeys [2], Jordi D'hondt [1] , Henri Devroey [2], Marc Juwet [1] and Eric Demeester [3]

[1]   KU Leuven Campus Technologiecampus, 9000 Gent, Belgium; Jordi.dhondt@kuleuven.be (J.D.); marc.juwet@kuleuven.be (M.J.)

[2]   KU Leuven Campus, 8200 Brugge, Belgium; kurt.claeys@kuleuven.be (K.C.); henri.devroey@kuleuven.be (H.D.)

[3]   KU Leuven Campus, 3590 Diepenbeek, Belgium; eric.demeester@kuleuven.be

*   Correspondence: sien.dieltiens@kuleuven.be

Abstract: Measuring lower extremity joint angles during cycling is interesting to derive joint loading from contact forces at the pedals and to determine the cause of cycling injuries. Traditionally, joint angles are determined in a stationary setup with high-resolution cameras that track marker movement in a lab environment. Alternatively, joint angles can be estimated mathematically in-situ: the lower extremities, bicycle frame and pedal arms are presented as a 5 bar linkage system which is fully defined by the lower extremity segment lengths, seat height and pedal position. As most instrumented pedals for power measurements include pedal orientation measurements, the bar linkage system demands no special equipment to derive joint loadings from pedal loads. The aim of this study is to validate the bar linkage system for joint angle estimation in the sagittal plane during in-situ cycling. Ten subjects cycled on a stationary bike while the hip, knee and ankle angles were measured with a Vicon optoelectronic motion capture system and simultaneously calculated with the bar linkage system. The results were averaged to subject-specific and method-specific ensemble average curves in the function of the phase in the pedal cycle and compared by a correlation analysis, Bland Altman plot, and Spm1D paired T-test. The hip and knee angle estimation of the bar linkage system showed no statistically significant difference from the optoelectronic system. Moreover, the ankle showed a statistically significant difference in the last half of the recovery phase of the pedal cycle. As the difference was maximally 3°, it has no clinical significance when deriving joint loading from contact forces at the pedal.

Keywords: bar linkage model; optoelectronic motion capture system; validation; kinematics; cycling

1. Introduction

Due to the addition of electrically powered pedal-assistance, increasingly more inactive people tend to cycle, with a greater chance on accidents [1]. Twisk et al., point out that electric bicycles are more effortful to stabilize, due to their higher center of gravity [2]. Longer cycling distances are covered, leading to an enlarged risk for cycling-related injuries by cause of overuse [3]. Cycling sores are often the result of a maladaptive cycling posture, cycling technique or bicycle geometry [4]. They are more commonly prevalent in the lower extremity [5] and can often be related to lower extremity joint kinematics and joint loading [6,7]. Joint loading can be derived from joint angles and contact forces in the seat or pedals [8]. Contact forces can easily be determined with instrumented pedals and seat posts [9,10] Traditionally, joint angles (and human motion in general) are determined with optoelectronic motion capture systems involving high-resolution infrared cameras that track reflective

markers attached to the body during movement [11]. The systems require a purpose-built laboratory with specially trained personnel and a stationary setup of the bicycle. As stationary cycling differs from in-situ cycling, more mobile and flexible alternatives are explored to measure joint angles [12]. Inertial Measurement Units combine gyroscopes and accelerometers in a compact module to determine acceleration, speed and position [13]. The position measurements show great potential, though up until now are affected by drift which makes them unstable for prolonged joint angle measurements during cycling [14]. Another alternative is a mathematical estimation by Hull and Jorge for which the lower extremities, bicycle frame and pedal arms are presented as a 5 bar linkage system. Joint angles are estimated in the sagittal plane based on the dimensions of the lower extremities, and the location of the seat and pedals [15]. This system makes a stationary setup superfluous, the cyclist can cycle outdoors, and there is no need for a lab environment. The bar linkage system is particularly interesting to calculate in-situ joint loading as pedal orientation measurements are often included in instrumented pedals [9] and no extra equipment is needed. The aim of this study is to validate the bar linkage system for joint angle estimation in the sagittal plane during in-situ cycling. Joint angles will be estimated with the bar linkage system and simultaneously measured with a validated optoelectronic motion capture system (VICON) for comparison.

2. Materials and Methods

2.1. Participants

Seven healthy males and three healthy females volunteered for this study. Before testing, subjects were informed about all the procedures of the study and an informed consent form was signed. The study is approved by the Ethical Committee research UZ/KU Leuven. The characteristics of the subjects can be found in Table 1.

Table 1. Subject characteristics.

|	Mean	Standard Deviation
Age (years)	26	2
Weight (kg)	65.83	15.63
Length (m)	1.73	0.19
BMI	22.00	0.35

2.2. Experimental Design

The subject's lower limb segment lengths are measured with high precision and reproducibility based on anatomic locations. Markers of a validated optoelectronic motion capture system (Vicon) are attached to the lower limbs according to the Lower Limb and Trunk Model of the Liverpool John Moores University [16,17]. The subjects cycle two sets of two minutes on a stationary bike with instrumentation to (i) estimate joint angles as a function of the lower limb segment lengths and the output data of the instrumentation, and (ii) record joint angles by marker tracking with the optoelectronic motion capture system.

2.3. Instrumentation

2.3.1. Bicycle Instrumentation

The bicycle is equipped with instrumentation to record pedal orientation. The pedal arm angle is determined by a unique encoder, including a toothed disk clamped over the crank and an optical sensor fixated on the frame (Figure 1a). The sensor counts the gabs, starting from a wider reference gab. The pedal angle is measured with unique instrumented pedals that measure pedaling loads with a maximal standard error percentage of the full scale of 0.5% (Figure 1b) [9]. The pedals contain a magnetometer and a diametrically polarized magnet on the pedal axis to determine the angle between

pedal and pedal arm. Taking the encoder values into account, the pedal angle relative to the horizontal position is defined.

(**a**)	(**b**)
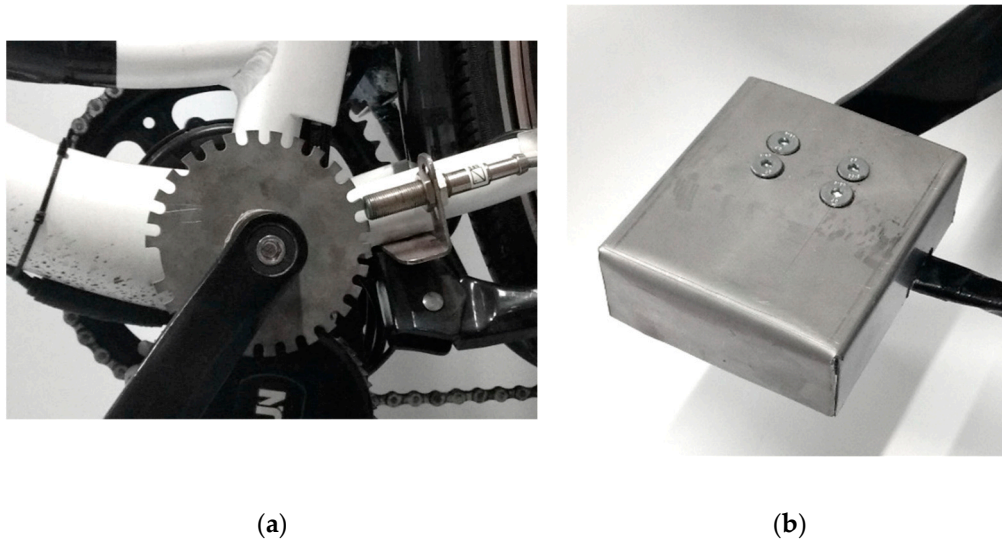
Figure 1. From left to right (**a**) unique encoder, (**b**) instrumented pedal.

2.3.2. Vicon Motion Capture System

A Vicon optoelectronic motion capture system is utilized to record human motion with a sample frequency of 100 Hz. It combines fourteen Vero cameras, a D-link power base for power distribution and a Vicon Lock+ for timecoding and synchronization with the instrumented bicycle. The cameras track 14 mm sphere pearl markers which are attached to the skin of the subject with Scotch 3M double-sided tape. In order to ensure maximal accuracy, a minimum of three cameras were needed to track a marker at any given time.

2.3.3. Data Acquisition and Synchronization

All data is recorded at a frequency of 100 Hz. The data acquisition system of the instrumented bicycle exists of a cDAQ-9178 chassis of National Instruments containing (i) a universal analogue input module NI9219 to measure the strain gauge output and (ii) a universal analogue input module NI9215 to measure the encoder values and to synchronize the data with an Arduino Micro. The magnetic rotary meter is connected to an Arduino Micro to measure pedal orientation. As the lock+ keeps running, while the cDAQ stops after every cycling set, the data needs to be synchronized. The Arduino sends out a varying signal to the cDAQ and to the Vicon Lock+ to add a unique high-low pattern. After the experiments, all data is shifted in time until it fully matches the unique high-low pattern of the Arduino.

2.4. Setup

The bicycle is installed stationary on a bicycle trainer, the seat height is measured and remains unchanged during all tests. An analogue output of the Arduino module is connected to an analogue input of the lock+ for post-test synchronization. The Vicon cameras are warmed up for 30 min, and all reflecting parts of the bicycle are covered. When the cameras are warm, and the room temperature is stable, the cameras are calibrated.

2.5. Protocol

Every subject is weighted, and lower limb lengths are notated. They are barefoot wearing only underwear. They are lying supine in the anatomical position. The feet point to the sealing with a maximally voluntarily dorsiflexion. Inner leg, thigh, shank, and mid-foot length were determined

with a tape measure (by measuring, respectively, the distance from the greater trochanter to the lateral malleolus, from the greater trochanter to the lateral femoral condyle, from the lateral femoral condyle to the lateral malleolus and from the medial malleolus to the os naviculare), as seen in Table 2. All anatomical locations are measured from the centers.

Table 2. References to determine segment lengths.

Segment	Link	Proximal Reference	Distal Reference
1	Thigh	Greater Trochanter	Lateral Femoral Epicondyle
2	Shank	Lateral Femoral Epicondyle	Lateral Malleolus
3	Mid-Foot	Medial Malleolus	Os Naviculare

Markers are attached to the naked skin according to the Lower Limb and Trunk Model of the Liverpool John Moores University [16,17]. The model considers eight segments: Two feet, two shanks, two thighs, the pelvis, and trunk. In total, 44 markers are applied to fully capture the torso and lower limb movement (Figure 2).
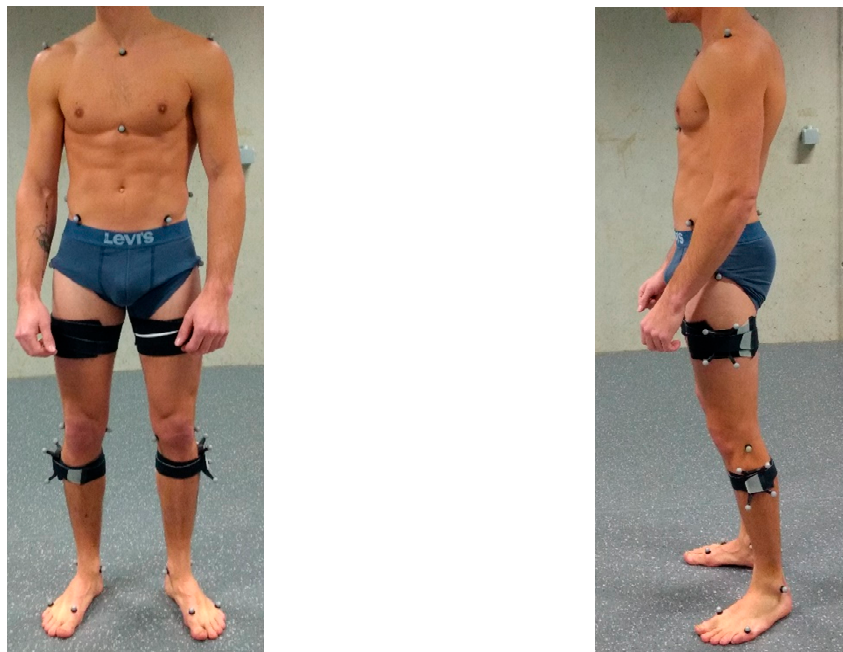
Figure 2. Marker placement.

A static trial is performed to record static marker locations: The subject stands still in the anatomical position, with slightly abducted arms. Functional knee and hip movements are performed to define the motion between the markers: The joints are separately moved through their full range of motion: Flexion/extension, abduction/adduction, internal/external rotation for the hip and flexion/extension for the knee. Markers are labelled, segments are described, and a subject-specific Lower Limb and Trunk Model is created to record joint motion. Every subject cycles two sets of 2 min on a self-selected relaxed tempo (Figure 3). The instrumented bicycle and the optical motion system are manually activated and post-test synchronized based on the timestamp of the Arduino.

The subjects are provided guidelines during the test: Cycling gear is fixed, both hands are at all times on the handlebar, and the buttocks on the seat. The bare feet are placed centrally on the pedals, pressing the metatarsal bones to the pedal surface. Before and after every cycling set, foot position is evaluated. Tests are filmed in the sagittal and frontal plane.

Figure 3. Test setup.

2.6. Angle Calculation

The leg-bicycle system is described as a bar linkage model with the frame as a fixed link and the crank, foot, shank and thigh as moving links. Figure 4 presents an overview of the system. Joint angles are determined according to the work of Hull and Jorge [15]. A schematic overview of the angles and segment lengths is presented in Figure 4. The ankle angle (γ), addressing the angle between the shank and mid-foot, is calculated as:

$$\gamma = \zeta + \varepsilon - \delta - \pi/2 \tag{1}$$

For which ζ is the angle between pedal and crank, ε is the crank angle relative to the vertical and δ is the angle between the mid-foot and the pedal.

The knee angle (β) and hip angle (α) are described in function of seven geometric constants.

$$\beta = tan^{-1}\left[\frac{(C-D) - l_t \sin\alpha}{(A-B) - l_t \cos\alpha}\right] \tag{2}$$

$$\alpha = -2\, tan^{-1}\left[\frac{2G \pm \left[(2G)^2 - 4(E+F)(E-F)\right]^{1/2}}{2(E+F)}\right] \tag{3}$$

For which l_t is the length of the shank and A, B, C, D, E, F and G are respectively given by Equations (4)–(10):

$$A = L2 + l_c\, cos\varepsilon \tag{4}$$

$$B = l_f\, cos\gamma \tag{5}$$

$$C = L1 + l_c\, sin\varepsilon \tag{6}$$
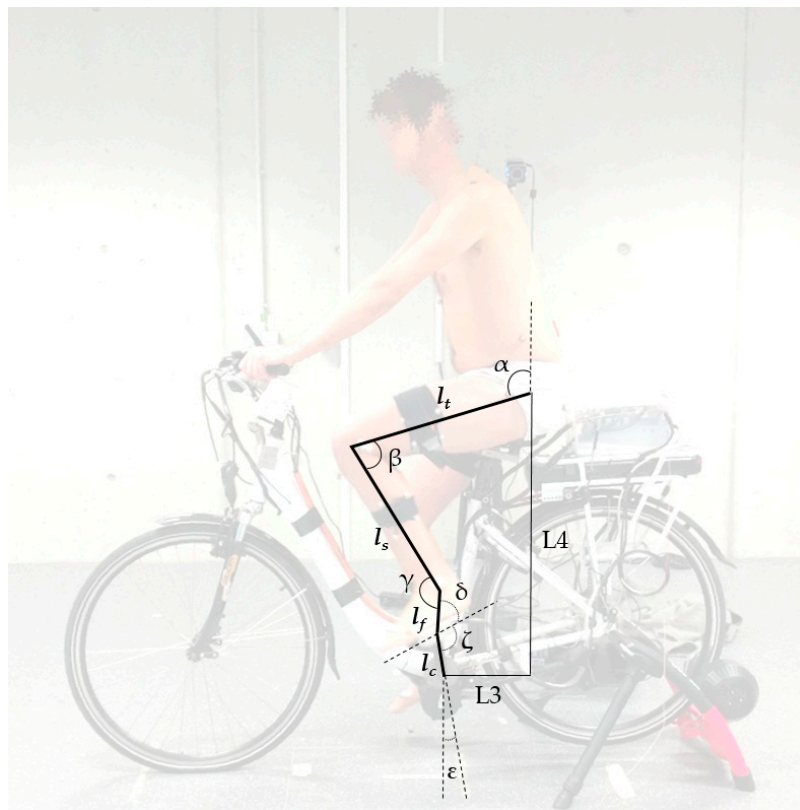
$$D = l_f sin\gamma \tag{7}$$

$$E = (A-B)^2 + (C-D)^2 + l_t^2 - l_s^2 \tag{8}$$

$$F = 2(A-B)l_t \tag{9}$$

$$G = 2(C-D)l_t \tag{10}$$

$L1$ and $L2$ are the horizontal and vertical distance between crank and seat, respectively. l_c, l_f, l_s and l_t are the crank, mid-foot, shank, and thigh length, respectively.

Figure 4. Schematic overview of the angles and segment lengths.

2.7. Statistical Analysis

Only constant cycling data is included in the analysis: A minimum of five consecutive pedal cycles needs to be counted, and the deviation between the encoder peaks should be less than 5%. The consistent cycles are averaged to ensemble average curves (AVCs), which are subdivided into subject-specific and method-specific AVCs. Subject-specific AVCs consider one AVC for every subject, for every joint, for every leg, for every measurement method, resulting in 120 subject-specific AVCs. Method-specific AVCs consider one AVC for every joint for every method, resulting in six method-specific AVCs in total. The original time scale is converted to a position within the pedal cycle ranging from 0 to 360 degrees. The pedal cycle considers four phases: The pushing phase when the pedal is in the upper dead center (0°), the pulling phase when the pedal is in the lower dead center (180°), the power phase when the pedal travels from the upper dead center to the lower dead center (0–180°) and the recovery phase when the pedal travels from the lower dead center to the upper one (180°–360°) [18]. As every phase has its own characteristics, data points of every phase are considered in the statistical analysis: Every 12 degrees, a value is saved—leading to 30 data points for one pedal cycle.

The AVCs of the bar linkage system and the optoelectronic motion capture system are plotted together and compared with each other by a paired *t*-test of Spm1d. Spm1d is a validated package for one-dimensional Statistical Parametric Mapping utilizing the random field theory [19]. It implements a non-sphericity correction in the *t*-test by adjusting the degrees-of-freedom using the Satterthwaite approximation from restricted maximum likelihood estimates of covariance components.

A correlation analyses is performed to measure the strength of a linear association between the two methods. All data points of the AVCs are utilized, resulting in a widespread sample with a considerable variating parameter, necessarily for correlation analysis. Pearson's coefficient of

determination (r^2) and the root-mean-square error (RMSE) are presented in the section results. A Bland and Altman (B&A) analysis is performed to evaluate a bias between the mean differences, and estimate an agreement interval, within which 95% of the differences of the second method.

3. Results

3.1. Method Specific AVCs

Method-specific AVCs are calculated, resulting in three AVCs (hip, knee and ankle) for the bar linkage system and three AVCs for the optical motion system.

3.1.1. Paired *t*-Test

For every joint, the two method-specific AVCs are plotted with their standard deviation in Figure 5.1a–5.3a. Figure 5.1 addresses the hip, 5.2 addresses the knee and 5.3 addresses the ankle. The results of an SPM paired-*t*-test is plotted in Figure 5.1b–5.3b.
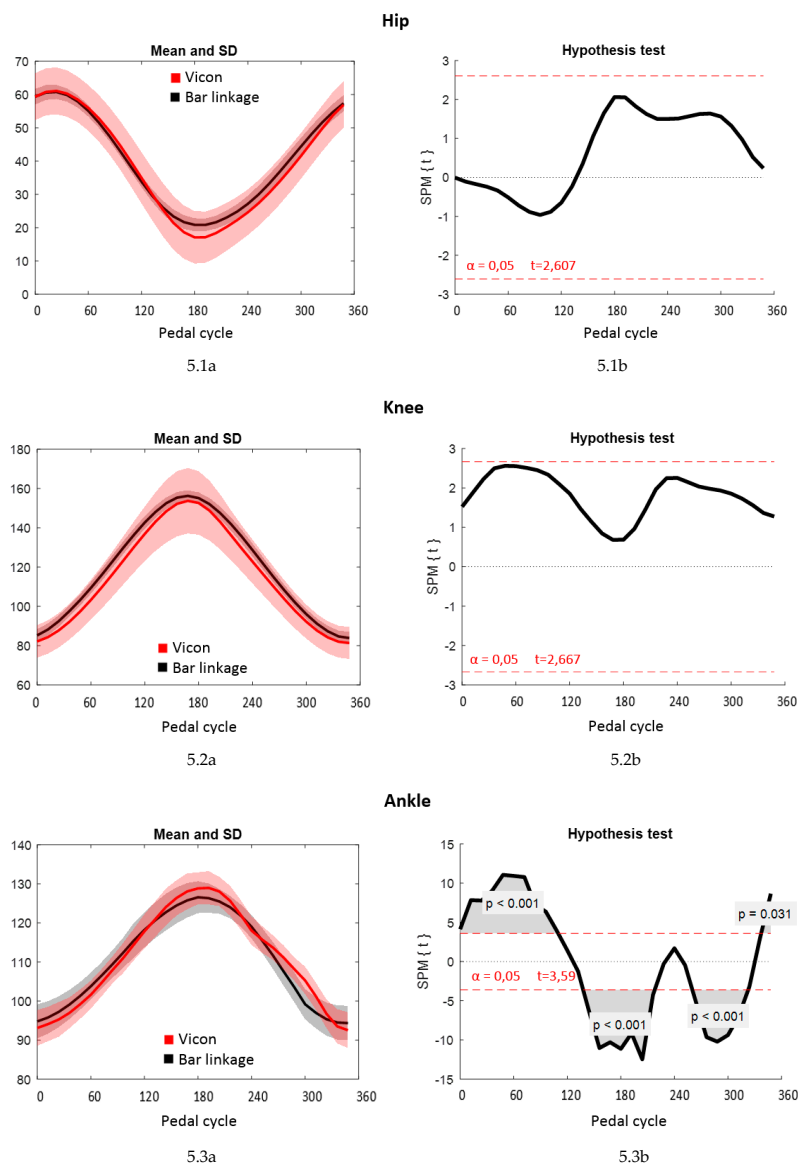

Figure 5. From top to bottom: SPM1D output of the method-specific AVCs from the hip (5.1); knee (5.2) and ankle (5.3). From left to right: Mean and standard deviation of the motion capture system and the bar linkage (**a**); plot of the *p*-values (**b**).

The largest difference for the hip is located in the region between 168° and 216°, though it is not significant ($\alpha = 0.05$, $t = 2.607$). The largest difference for the knee is located in the region of 36–96° and of 192–276°, though are not significant ($\alpha = 0.05$, $t = 2.667$). The ankle has three zones with a significant difference ($\alpha = 0.05$, $t = 3.59$, $p < 0.001$) located in the region of 336–108°, 144–216°, and 264–312°.

3.1.2. Correlation and Bland Altman

For every joint, the correlation between the two method-specific AVCs is plotted in Figure 6.1a–6.3a. Figure 6.1 addresses the hip, Figure 6.2 addresses the knee, and Figure 6.3 addresses the ankle. The B&A analyses plot the difference between the two methods in function of the mean of the two methods. The results are presented in Figure 6.1b–6.3b.
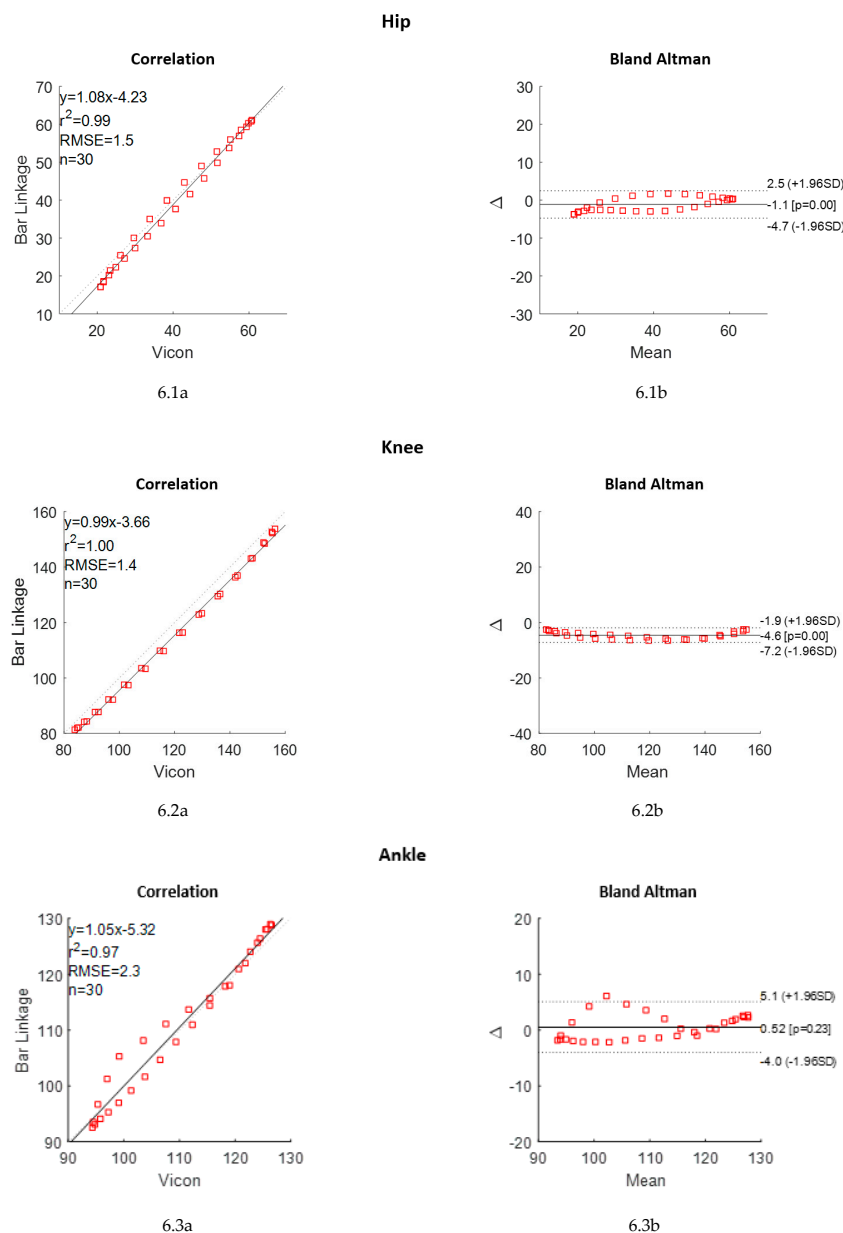
Figure 6. From top to bottom: Correlation and B&A analysis of method-specific AVCs for the hip (6.1); knee (6.2) and ankle (6.3). From left to right: Correlation plot (**a**); B&A plot (**b**).

The hip, knee and ankle show a very high correlation with r^2 values of 0.99, 1, and 0.97, respectively, and RMS values of respectively 1.5, 1.4, and 2.3. The B&A plot of the ankle presents one outlier that is

not within the margins of 1.96 times the standard deviation. All values of the knee and hip are within the margins.

3.2. Subject-Specific AVCs

Subject-specific AVCs are calculated, resulting in 60 AVCs covering the joints (left hip, right hip, left knee, right knee, left ankle and right ankle) of every subject for the bar linkage system and for the optical motion system.

3.2.1. Correlation Analysis

Table 3 presents the maximal and minimal values found between all subjects for the six joints. The difference between the left and right joint is marginal. r^2 is situated between 0.963 and 0.996 for the hips, between 0.999 and 0.983 for the knees and between 0.919 and 0.981 for the ankles with $n = 30$ and $p < 0.001$. The r^2 presents the smallest variation for the knees, followed by the hips and the Ankles. The RMSE is situated between 0.907 and 2.879 for the hips, between 0.530 and 3.500 for the knees and between 0.979 and 3.409 for the ankles, with the smallest variation for the hips, followed by the ankles and the knees.

**Table 3.** Outcome subject-specific correlation analysis.

	Left Hip	Right Hip	Left Knee	Right Knee	Left Ankle	Right Ankle
r^2 minimal	0.963	0.972	0.983	0.984	0.922	0.919
r^2 maximal	0.996	0.996	0.999	0.999	0.979	0.981
RMSE minimal	0.907	1.041	0.725	0.530	0.979	1.746
RMSE maximal	2.879	2.467	3.500	3.396	3.409	3.318

3.2.2. Bland Altman

Table 4 and Figure 7 display the number of subjects with outliers for the six joints in the function of the pedal cycle. All ten subjects present no outliers for the left and right hip. Six out of ten and seven out of ten subjects present no outliers for the left and right knee, respectively. The outliers are found in the region of 156–180° for the left knee, and 168–192° for the right knee. Five out of ten and four out of ten subjects present no outliers for the left and right ankle, respectively. The outliers are found in the region of 300–312°. All outliers are found in the region between 1.97 times the standard deviations and 2.12 times the standard deviation.

Table 4. Outcome subject-specific B&A analysis.

	Left Hip	Right Hip	Left Knee	Right Knee	Left Ankle	Right Ankle
Subject-specific AVCs without outliers	10	10	6	7	5	4
Subject-specific AVCs with outliers $x (y) = x$ subjects present an outlier at location y	0	0	2 (156°) 4 (168°) 4 (180°)	2 (168°) 3 (180°) (1 (192°)	5 (300°) 2 (312°)	6 (300°) 4 (312°)
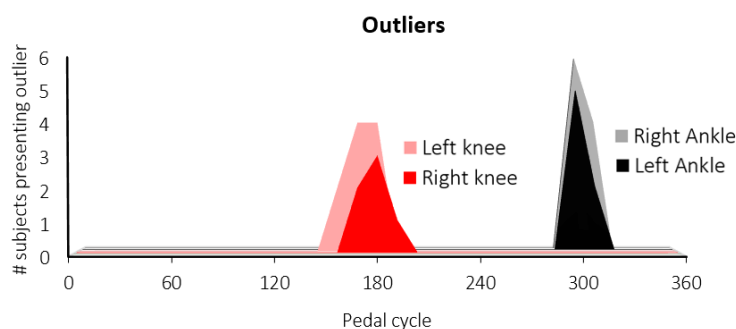
Figure 7. Visual comparison of the number of subjects with outliers for a certain joint in function of the pedal cycle.

4. Discussion

4.1. Method Specific AVCs

4.1.1. Paired *t*-Test

Regarding the hip, a maximal difference of 3° can be detected visually when the pedal enters the pushing phase of the pedal cycle, though this is statistically not significant. It has, furthermore, no clinical relevance as it is relatively small compared to the full range of motion of the hip during cycling of 41°. Regarding the knee, a constant overestimation of 3° is viewed, though it is not large enough to be statistically significant. The full range of motion of the knee is 72° during cycling, an overestimation of 3° has no clinical relevance. The ankle presents three regions with statically relevant differences. A maximal overestimation of 2° is detected in the pushing phase, and a maximal underestimation of 3° is detected in the pulling phase. Additionally, the curve displays an extra peak in the last half of the recovery phase. This is statistically significant, though, for a full range of motion of 34°, it has no clinical relevance. The bar linkage system presents a lower standard deviations, which could suggest it is a more stable measuring method. The standard deviation of the bar linkage system is the largest for the ankle, followed by the knee and the hip. This can be related to the size of the movement: The larger the movement, the smaller the standard deviation. For the optoelectronic motion capture system, the largest standard deviation is found for the knee, followed by the hip and at last the ankle. The standard deviation of the optoelectronic motion capture system for the knee and hip is significantly higher than for the bar linkage system. This can be caused to the placement of the markers needed to determine the movement. The knee and hip present a higher wobbling mass and more soft tissue artefacts than the slender ankle. This could suggest that the bar linkage system is a more stable measuring method for voluptuous cyclists.

4.1.2. Correlation and B&A Analysis

All joint angles present a very high correlation for the two methods. A high correlation is required to validate a method—though a high correlation does not necessarily imply that the examined method is a good substitution for the golden standard. Bland and Altman point out that a high correlation essentially implies that the sample is widespread, considering (i) the measuring interval affects r and r2 without affecting the agreement and (ii) a change in the scale of measurement significantly affects the agreement without affecting the correlation analysis [20]. The B&A analysis is performed to evaluate the bias between the two methods. It reveals one significant outlier for the ankle located at 300°, confirming the results of the Spm1D analysis. The ankle's overestimation in the pushing phase and the underestimation in the pulling phase is not found back in the B&A analysis as these values still fall between the margins of 1.96 times the standard deviation.

4.2. Subject-Specific AVCs

All subjects present a similar correlation with a marginal difference between the left and right leg. The correlation of the subject-specific AVCs are analogues to the method-specific AVCs. Regarding the B&A analysis, more outliers are found when the bar linkage system and the optical motion system are compared to the level of the subjects. The subject-specific AVCs of the hips present the same outcome as the method-specific AVC. The subject-specific AVCs of the knee present a different outcome, namely, for 35% of the subjects one or two outliers are discovered in the pulling phase. This could suggest that the averaging ensemble technique has hidden some erroneous data for the knee in the pulling phase. Though, the difference is very small: In 35% of the cases one or two outliers are found located only slightly outside the confident interval (at maximal 2.12 times the standard deviation instead of 1.96 times the standard deviation). Regarding the ankle, 55% of the subjects present one or two outliers in the second half of the recovery phase, which is in line with the method-specific AVC B&A analysis.

4.3. Limitations and Future Directions

The bar linkage system proved to deliver accurate joint angle calculation on bicycles, though some limitations should be considered. The angles are a projection in the sagittal plane of the flexion and extension, not taking the lateral and medial rotation into account. Furthermore, possible hip and feet movement was neglected as the cyclist was forced in a certain setup. Subsequently, the influence of hip and feet movement, different hip and feet setups should be studied. In future work, the bar linkage system will be utilized on a fully instrumented city bike for woman with pedal power assistance to derive in-situ joint loading from contact forces in the seat and pedals to analyze the influence of pedal power assistance on joint kinetics.

5. Conclusions

The bar linkage system proved to be a good estimator of the lower limb joint angles in the sagittal plane during cycling. A very strong correlation is found between the bar linkage system and the optoelectronic motion capture system for all the joints of every subject. The B&A analysis of the AVCs from the hip angles presented no outliers, and the t-test revealed no significant differences. The B&A analysis of method-specific AVCs from the knee angles presented no outliers, subject-specific AVCs from the knee angles presented a marginal amount. Furthermore, the t-test of the method-specific AVCs presented no significant difference between the two methods. The B&A analysis of the ankle presented one outlier in the second half of the recovery phase for the method-specific AVCs and maximally two outliers for the subject-specific AVCs in the same region. The t-test confirmed these results and additionally revealed a statistically significant overestimation in the pushing phase and underestimation in the pulling phase of 3°. Because a difference of 3° has no clinical relevance when discussing joint angles to determine joint loading, the bar linkage system is seen as a good alternative for optoelectronic motion capture systems to capture cycling movement. It can measure joint angles while cycling in-situ, and therefore, does not require a lab environment, can be measured with traditional instrumented pedals, and is not affected by wobbling mass and soft tissue artefacts of the lower limbs.

Author Contributions: Conceptualization, S.D.; Data curation, S.D., J.D. and H.D.; Formal analysis, S.D.; Investigation, S.D.; Methodology, S.D., K.C. and H.D.; Project administration, S.D., K.C. and E.D.; Resources, M.J.; Software, S.D., J.D. and H.D.; Supervision, K.C., M.J. and E.D.; Validation, S.D., K.C. and M.J.; Visualization, S.D.; Writing—original draft, S.D.; Writing—review & editing, K.C. and E.D. All authors have read and agreed to the published version of the manuscript.

References

1. Schepers, P.; Fishman, E.; Hertog, P.D.; Wolt, K.K.; Schwab, A.L. The safety of electrically assisted bicycles compared to classic bicycles. *Accid. Anal. Prev.* **2014**, *73*, 174–180. [CrossRef] [PubMed]
2. Twisk, D.; Platteel, S.; Lovegrove, G. An experiment on rider stability while mounting: Comparing middle-aged and elderly cyclists on pedelecs and conventional bicycles. *Accid. Anal. Prev.* **2017**, *105*, 109–116. [CrossRef] [PubMed]
3. Visentini, P. A systematic review of parameters related to cycling overuse injuries or pain. *J. Sci. Med. Sport* **2017**, *20*, e69–e70. [CrossRef]
4. Callaghan, M.J. Lower body problems and injury in cycling. *J. Bodyw. Mov. Ther.* **2005**, *9*, 226–236. [CrossRef]
5. Bernardo, N.; Barrios, C.; Vera, P.; Laiz, C.; Hadala, M. Incidence and risk for traumatic and overuse injuries in top-level road cyclists. *J. Sports Sci.* **2012**, *30*, 1047–1053. [CrossRef] [PubMed]
6. Heijink, A.; Gomoll, A.H.; Madry, H.; Drobnič, M.; Filardo, G.; Mendes, J.E.; Van Dijk, C.N. Biomechanical considerations in the pathogenesis of osteoarthritis of the knee. *Knee Surg. Sports Traumatol. Arthrosc.* **2011**, *20*, 423–435. [CrossRef] [PubMed]

7. Miyazaki, T.; Wada, M.; Kawahara, H.; Sato, M.; Baba, H.; Shimada, S. Dynamic load at baseline can predict radiographic disease progression in medial compartment knee osteoarthritis. *Ann. Rheum. Dis.* **2002**, *61*, 617–622. [CrossRef] [PubMed]

8. Redfield, R.; Hull, M. On the relation between joint moments and pedalling rates at constant power in bicycling. *J. Biomech.* **1986**, *19*, 317–329. [CrossRef]

9. Sien, D.; D'Hondt, J.; Juwet, M.; Versteyhe, M. development of a low-cost measurement system to determine 3-Dimensional pedal loads during in-situ cycling. *Transp. Probl.* **2019**, *14*, 151–160. [CrossRef]

10. Sien, D.; Jordi, D.; Juwet, M.; Shariatmadar, K.; Versteyhe, M. Design and calibration of an instrumented seat post to measure sitting loads while cycling. *Sensors* **2020**, *20*, 1384. [CrossRef] [PubMed]

11. Bini, R.R.; Dagnese, F.; Da Rocha, E.S.; Silveira, M.C.; Carpes, F.P.; Mota, C.B. Three-dimensional kinematics of competitive and recreational cyclists across different workloads during cycling. *Eur. J. Sport Sci.* **2016**, *16*, 1–7. [CrossRef] [PubMed]

12. Mesquita, I.; Fonseca, P.; Pinheiro, A.R.V.; Correia, M.; Silva, C. Methodological considerations for kinematic analysis of upper limbs in healthy and poststroke adults Part II: A systematic review of motion capture systems and kinematic metrics. *Top. Stroke Rehabil.* **2019**, *26*, 464–472. [CrossRef] [PubMed]

13. Cordillet, S.; Bideau, N.; Bideau, B.; Nicolas, G. Estimation of 3D knee joint angles during cycling using inertial sensors: Accuracy of a novel sensor-to-segment calibration procedure based on pedaling motion. *Sensors* **2019**, *19*, 2474. [CrossRef] [PubMed]

14. Feng, Y.; Li, X.; Zhang, X. An adaptive compensation algorithm for temperature drift of micro-electro-mechanical systems gyroscopes using a strong tracking kalman filter. *Sensors* **2015**, *15*, 11222–11238. [CrossRef] [PubMed]

15. Hull, M.; Jorge, M. A method for biomechanical analysis of bicycle pedalling. *J. Biomech.* **1985**, *18*, 631–644. [CrossRef]

16. Vanrenterghem, J.; Gormley, D.; Robinson, M.; Lees, A. Solutions for representing the whole-body centre of mass in side cutting manoeuvres based on data that is typically available for lower limb kinematics. *Gait Posture* **2010**, *31*, 517–521. [CrossRef] [PubMed]

17. Robinson, M.A.; Vanrenterghem, J. An evaluation of anatomical and functional knee axis definition in the context of side-cutting. *J. Biomech.* **2012**, *45*, 1941–1946. [CrossRef] [PubMed]

18. Timmer, C.A.W. Cycling biomechanics: A literature review. *J. Orthop. Sports Phys. Ther.* **1991**, *14*, 106–113. [CrossRef] [PubMed]

19. Pataky, T.; Vanrenterghem, J.; Robinson, M.A. Zero- vs. one-dimensional, parametric vs. non-parametric, and confidence interval vs. hypothesis testing procedures in one-dimensional biomechanical trajectory analysis. *J. Biomech.* **2015**, *48*, 1277–1285. [CrossRef] [PubMed]

20. Bland, J.M.; Altman, D.G. Measuring agreement in method comparison studies. *Stat. Methods Med. Res.* **1999**, *8*, 135–160. [CrossRef] [PubMed]